

Article

Finite Frequency H_∞ Control for Doubly Fed Induction Generators with Input Delay and Gain Disturbance

Shaoping Wang , Jun Zhou and Zhaoxia Duan

College of Energy and Electrical Engineering, Hohai University, Nanjing 211100, China

* Correspondence: shaopingking@163.com

Abstract: Due to the rapid development of wind power, the stable operation of doubly fed induction generators (DFIGs) has attracted much attention. This paper focuses on the finite frequency (FF) H_∞ control for the DFIG with input delay, aiming to reduce the effects of current harmonic interferences and gain disturbances on the DFIG and improve the stability of the system. First, a DFIG state-space model with input delay under current harmonics was constructed. Second, based on the DFIG state-space model, an FF H_∞ state-feedback controller was designed from the frequency domain perspective, which makes the DFIG stable and robust against harmonic interferences and gain disturbances. Third, via the generalized Kalman–Yakubovich–Popov (GKYP) lemma and the Lyapunov theory, the FF H_∞ performance was evaluated in the form of linear matrix inequalities (LMIs), and then the state feedback FF H_∞ controller was designed. Finally, the simulation results showed the efficiency of the proposed approach.

Keywords: doubly fed induction generator; finite frequency domain; input delay; gain disturbance; H_∞ performance



check for updates

Citation: Wang, S.; Zhou, J.; Duan, Z. Finite Frequency H_∞ Control for Doubly Fed Induction Generators with Input Delay and Gain Disturbance. *Sustainability* **2023**, *15*, 4520. <https://doi.org/10.3390/su15054520>

Academic Editor: Hua Li

Received: 24 January 2023

Revised: 15 February 2023

Accepted: 16 February 2023

Published: 2 March 2023



Copyright: © 2023 by the authors. Licensee MDPI, Basel, Switzerland. This article is an open access article distributed under the terms and conditions of the Creative Commons Attribution (CC BY) license (<https://creativecommons.org/licenses/by/4.0/>).

1. Introduction

With the heavy consumption of fossil fuels, the quick depletion of natural resources and the severe deterioration of the environment, the exploration and deployment of clean and renewable energies has become urgent for sustainable economies [1]. Wind energy has attracted global attention since it is recyclable and does not pollute the ecological environment [2]. Wind power has the advantages of a wide abundance of reserves, high utilization rates and small land occupation [3]. Due to the transmission protocol and transmission environment, the signal transmission of DFIGs usually produces a time delay. The time delay is always present in the control and feedback channels of wind turbines because of the time required for the feedback digital controller to calculate and transmit, as well as unpredictable events during transmission (slowing down of data transmission due to temperature variations and electromagnetic interference). Studies show that small delays may hamper the control effects and even destabilize wind turbine systems [4].

Among wind systems, doubly fed induction generators (DFIGs) are low-cost and high-efficiency by virtue of constant frequency and variable speed advantages, and they are the mainstream type of wind turbines at present. The power quality is strongly influenced by the wind power grid connection. (1) Power electronics used in DFIG systems may cause harmonic pollution and affect the power quality. (2) The randomness of the wind speed in the wind farm causes changes in the output power, resulting in inevitable fluctuations and flicker in the voltage. (3) The intermittent wind power may lead to severe grid frequency fluctuations, which affects the power quality. In DFIG-based wind farms, DFIGs cannot ignore time delay in their input. In [5], considering time delay uncertainties in wind turbines, a multi-delay stabilization via the Casimir function was developed. In [6], a compensator was installed to overcome time delay effects. In [7], in the small disturbance stability sense, wind power stabilization was constructed, and sufficient criteria were obtained.

Practical signals only have finite frequency features; for example, seismic waves emerge only in the frequency interval (0.3,8) Hz, while human acoustic perception is most sensitive over (4,8) Hz. By [8], finite frequency (FF) current harmonics are associated with the stator itself, rotor converter and grids. In [9], when three-phase grid voltages are unbalanced, the grids will generate stator negative sequence voltage and current. However, most control strategies for DFIGs are contrived commonly in the entire frequency (EF) domain sense [10]. This brings in high conservatism in controller parametrization, which leads to low robustness under FF harmonics.

To cope with the delay and gain disturbances, various control strategies are employed, including adaptive [11], sliding mode [12], model predictive [13], and H_∞ optimal [14]. In particular, H_∞ control has been intensively considered for wind turbines for stability robustness and disturbance attenuation. For practical DFIGs, the limitation of microprocessor memory and word length, as well as A/D and D/A conversion errors, may cause the control to be inaccurate. This gain disturbance can easily lead to the destruction of the closed-loop system stability and performance degradation. Though remarkable theories have been established in the FF sense, few works are specified for DFIGs. Therefore, it is still substantial and challenging to deal with DFIG control in the FF sense.

This paper addresses the H_∞ control for a single DFIG with input delay under FF current harmonics interference and gain disturbance. More precisely, the H_∞ index is used to evaluate current harmonics and gain disturbance. By exploiting the generalized Kalman–Yakubovich–Popov (GKYP) lemma, the performance indices are converted into LMIs, and controller parametrization is solved by means of LMI feasible solution. In brief, this study contributes a novel type of FF control for the wind turbine DFIG with input delay under controller gain disturbances and current harmonics. Through the GKYP lemma and the Lyapunov theory, the FF H_∞ performance is transformed into linear matrix inequalities (LMIs) to facilitate the design of FF controllers with input delay. It has not been fully considered in previous studies on the control of the wind turbine DFIG. Moreover, a sufficient condition is presented to design the optimal FF controller for the DFIG.

The suggested H_∞ control improves robustness against time delay and gain disturbances, in comparison to those by EF control ones.

Notations: For a matrix M , its transpose, inverse and orthogonal complements are denoted by M^T , M^{-1} and M^\perp , respectively. $M^H = \overline{M}^T$ means conjugate transpose. $M^T = M > 0$ means that the symmetric matrix M is positive. Given a square matrix P , $\text{He}(P) = P + P^T$. I_n denotes the $n \times n$ identity matrix. R and C denote the real and complex number sets, respectively. $\mathbf{R}^{n \times m}$ and $\mathbf{C}^{n \times m}$ denote the set of all real and complex matrices of dimension $n \times m$, respectively. Also, $*$ denotes the transposed element in the symmetric position.

2. Preliminaries and Problem Formulation

A wind power system with a doubly fed induction generator (DFIG) is sketched in Figure 1. Accordingly, the DFIG-based wind turbine system consists of a windmill, a gearbox, a doubly fed induction generator, a slip ring and a converter. Electrically, the DFIG stator is directly connected to a power grid and the rotor is connected to the power grid through a converter. The rotor side provides the excitation current with adjustable amplitude, phase and frequency. The intermediate converter is in the form of two back-to-back PWMs that can achieve four-quadrant operation. The DFIG has the advantages of variable speed and constant frequency such that maximum energy tracking and grid frequency synchronism under wind fluctuations can be achieved simultaneously. In principle, doubly fed means that the stator and rotor of the induction generator are connected to the power grid and thus both of them can create energy exchanges with the power grid. To realize doubly fed operations, PWM inverters are installed on the generator side, which make the rotor excitation flexible and fasten the power exchange [15].

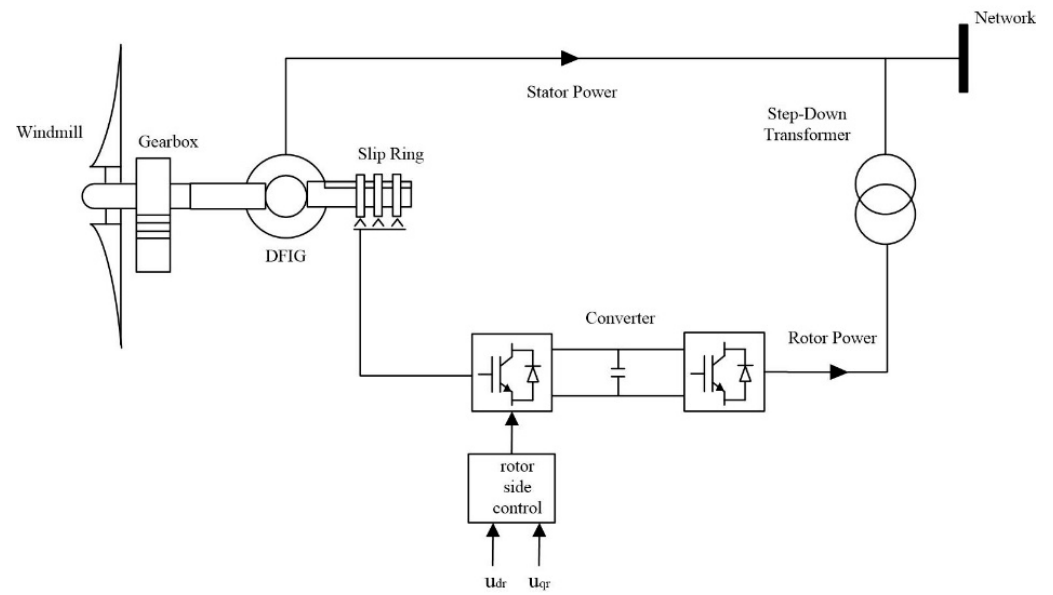


Figure 1. Scheme of a DFIG-based wind turbine system.

2.1. Electromechanical Transient Modeling of DFIG

To model the electromechanical transient of the DFIG in the steady state, it is assumed that the steady state electromechanical transient is much slower than those of the electronic switching in devices such as the converters. Hence, it is reasonable to say that the switching dynamics of the electronic devices have died out where the electromechanical transience of the DFIG in the steady state is concerned. Together with DC capacitor voltage dynamics of the rotor being neglected, the steady state equivalent circuit of the DFIG is given in Figure 2.

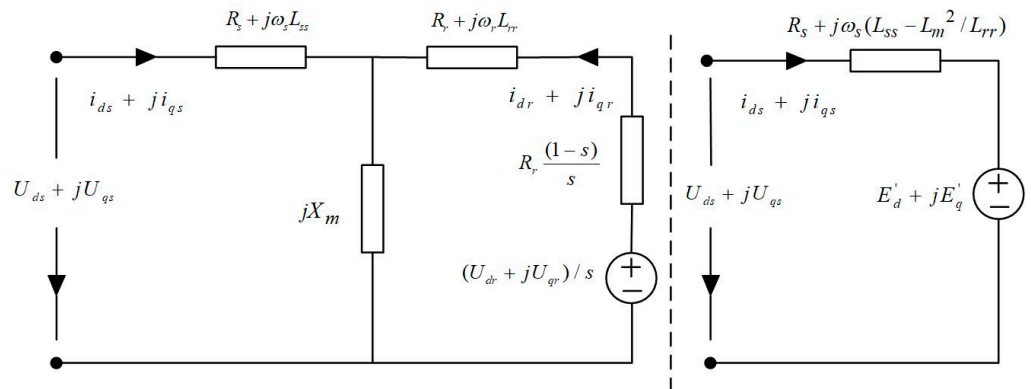


Figure 2. Dynamic equivalent circuit of the DFIG wing turbine system.

As denoted in Figure 2, the subsequent notations are adopted throughout the paper. s is the rotor slip rate; L_{ss} and L_{rr} are the stator and rotor self-inductances, respectively; L_m and X_m are the mutual inductance and reactance, respectively; R_r and R_s are the rotor and stator resistances, respectively; ω_s and ω_r are the synchronous angular velocity and rotor angular velocity, respectively; $U_{ds}(U_{dr})$ and $U_{qs}(U_{qr})$ are the d - and q - shaft stator (rotor) voltages, respectively; E_d' and E_q' are d - and q - shaft rotor voltages under the sub-transient, respectively; $i_{ds}(i_{dr})$ and $i_{qs}(i_{qr})$ are the d - and q - shaft stator (rotor) currents, respectively. In the above and what follows, the time variable t is dropped for simplicity.

The electromechanical transient of the DFIG in the steady state sense can be modeled as a third-order equation and its corresponding power equations:

$$\begin{cases} 2H \frac{d\omega_r}{dt} = T_m - T_e \\ \frac{dE'_d}{dt} = -\frac{1}{T'_{q'}} [E'_d - (L - L')i_{qs}] + s\omega_s E'_q - \frac{L_m}{L_{rr}} u_{qr} \\ \frac{dE'_q}{dt} = -\frac{1}{T'_{d'}} [E'_q + (L - L')i_{ds}] - s\omega_s E'_d + \frac{L_m}{L_{rr}} u_{dr} \\ P_s = T_e = E'_d i_{ds} + E'_q i_{qs} \\ Q_s = E'_d i_{ds} - E'_q i_{qs} \end{cases} \quad (1)$$

where H is the inertia time constant of the wind turbine as a single mass point model. $T_m = F\omega_r$ and T_e are the mechanical and electromagnetic torques on the generator rotor; F is the force acting on the mechanical torque.

Due to the widespread use of power electronics technology, most of the current AC excitation power supplies of DFIGs use two back-to-back PWM converters. The dual PWM converters contain a net-side converter and a rotor-side converter. However, because of the small capacity of the DFIG exciter converter, the control capability of the whole wind turbine is weak. There are mainly field-oriented control (FOC), also called vector control (VC), and direct torque control (DTC) for the DFIG control system, currently. In this paper, the rotor-side converter of the wind turbines adopts the vector control strategy [16,17]. The rotor voltage control equation is:

$$\begin{cases} u_{dr} = R_r i_{dr} + \sigma L_{rr} \frac{di_{dr}}{dt} - \omega_s \sigma L_{rr} i_{qr} \\ u_{qr} = R_r i_{qr} + \sigma L_{rr} \frac{di_{qr}}{dt} + \omega_s \left(\frac{L_m}{L_{ss}} \psi_s + \sigma L_{rr} i_{dr} \right) \end{cases} \quad (2)$$

where $\sigma = 1 - \frac{L_m^2}{L_{ss}L_{rr}}$.

It can be seen in (1) and (2) that if the rotor excitation power in the DFIG can be exploited as a voltage source, by controlling the rotor excitation voltages u_{dr} and u_{qr} , while the sub-transient voltages E'_d and E'_q can be modified to achieve the DFIG power control objectives.

2.2. Linearization and State–Space Remodeling of DFIG

The equations in (1) and (2) together are nonlinear differential algebraic ones, whose analytical solution is not directly available. In other words, if Equations (1) and (2) are directly used for FF controller design, it will involve a large number of numerical integrations in controller parametrization, which will greatly reduce the operating speed of the controller. Therefore, the nonlinear differential equations need to be linearized in advance.

In (1), we rewrite $\omega_r = 1 - \omega_s$, selecting the operating point $(\omega_{r0}, i_{ds0}, i_{qs0}, E_{d0}', E_{q0}')$. Then, we select $\Delta\omega_r, \Delta E'_d, \Delta E'_q$ as state variables, $\Delta\omega_r, \Delta P'$ and $\Delta Q'$ as output measurements, u_{dr} and u_{qr} as input control actions. Due to the power electronic devices in the DFIG, switching harmonics are inevitable. Any distortion of the control waveform will be coupled to the stator side as harmonics [18]. Assuming the current harmonic of the stator i_{ds} and i_{qs} are viewed as disturbances. The linearized state–space model for the DFIG is

$$\begin{cases} \dot{x}(t) = Ax(t) + B_1 p(t) + B_2 u(t) \\ y(t) = Cx(t) + Du(t) \end{cases} \quad (3)$$

and

$$\left\{ \begin{array}{l} A = \begin{bmatrix} -\frac{F}{2H} & -\frac{i_{ds0}}{2H} & -\frac{i_{qs0}}{2H} \\ -E'_{q0} & -\frac{1}{T_{0'}} & 1 - \omega_{r0} \\ E'_{d0} & \omega_{r0} - 1 & -\frac{1}{T_{0'}} \end{bmatrix} \in \mathbf{R}^{3 \times 3}, B_1 = \begin{bmatrix} 0 & 0 \\ 0 & \frac{L-L'}{T_{0'}} \\ -\frac{L-L'}{T_{0'}} & 0 \end{bmatrix} \in \mathbf{R}^{3 \times 2}, \\ B_2 = \begin{bmatrix} 0 & 0 \\ 0 & -\frac{L_m}{L_{rr}} \\ \frac{L_m}{L_{rr}} & 0 \end{bmatrix} \in \mathbf{R}^{3 \times 2}, C = \begin{bmatrix} 1 & 0 & 0 \\ 0 & i_{ds0} & i_{qs0} \\ 0 & -i_{qs0} & i_{ds0} \end{bmatrix} \in \mathbf{R}^{3 \times 3}, D = 0. \end{array} \right.$$

2.3. Input Time Delay and Gain Disturbance in DFIG

The time delay in signal processing always exists in the state-space Equation (3). More specifically, feedback digital controllers require time to calculate and transmit, so the time delay is not simply avoidable. In this study, to improve the robustness of the DFIG against input delay, a memoryless state-feedback control (4) was applied to suppress current harmonics in the rotor current $p(t)$ of (3).

$$u(t) = (K + \Delta K(t))x(t - \tau), t \in [0, \infty) \quad (4)$$

where $0 < \tau < \tau_m$ is input time delay $K \in \mathbf{R}^{2 \times 3}$ is the static gain matrix to be designed, and $\Delta K \in \mathbf{R}^{2 \times 3}$ is gain disturbance caused during implementation but in the form of

$$\Delta K(t) = RU(t)TK \quad (5)$$

where $R \in \mathbf{R}^{3 \times 1}$ and $T \in \mathbf{R}^{1 \times 2}$ are the real constant, and $U(t) \in \mathbf{R}$ is an unknown time varying continuous scalar function that satisfies $U^2(t) = U(t)^T U(t) \leq I$.

Hence, the closed-loop system of the DFIG with the controller (4) is given by

$$\begin{cases} \dot{x}(t) = Ax(t) + B_1 p(t) + B_2 (K + \Delta K)x(t - \tau) \\ y(t) = Cx(t) + D(K + \Delta K)x(t - \tau) \end{cases} \quad (6)$$

In particular, when neglecting the gain disturbance ΔK , the transfer function from $p(t)$ to $y(t)$ is denoted by $G_{py}(s, K)$ and given by

$$G_{py}(s, K) = (C + e^{-\tau s}DK)(sI_3 - A - e^{-\tau s}B_2K)^{-1}B_1 \in \mathbf{C}^{3 \times 2} \quad (7)$$

where I_3 stands for the 3×3 identity matrix.

2.4. FF Performance Specification for DFIGs

In the frequency domain, signals can be represented by several finite or infinite frequency trigonometric functions, which follow from the Fourier transform or generally the spectrum transform. For energy signals in power systems, the energy spectra are concentrated in some FF fashions. PWM is widely used in DFIGs, which includes harmonics in the air-gap magnetic field of the induction generator. One can impose some sinusoidal excitation voltage on the excitation circuit, and from the obtained spectra, the current harmonics are mainly in the frequency range of (250,550) Hz, as explained in [8]. In [9], it was also found that the DFIG frequency spectra of the output waveform are mainly concentrated around the integer multiplications of the switching frequency f_s such as $2f_s$, $3f_s$, etc. With respect to the (2,4) kHz converter switching frequency, external current harmonics to the DFIG are mainly around (2,8) kHz. In [19,20], specifications of grid harmonics are summarized among (50,150) Hz. Therefore, if FF features of switching and disturbances are not taken into account in H_∞ control, no practical optimal performance in the DFIG can be obtained.

$$\Omega_d = \{\omega \in \mathbf{R} | (\omega - \omega_1)(\omega - \omega_2) \leq 0\} = [\omega_1, \omega_2] \quad (8)$$

where $\omega_2 > 0$ and $\omega_1 > 0$ are the upper and lower bounds for frequencies in harmonic interference and disturbance, respectively. Now we are ready to introduce the finite frequency (FF) performance for our later use.

Definition 1. Considering the system (6), the FF H_∞ performance index of $G_{py}(s, K)$ is

$$\|G_{py}(j\omega, K)\|_{\infty}^{\Omega_d} := \sup_{\omega \in \Omega_d} \bar{\sigma}[G_{py}(j\omega, K)] > 0$$

where $\bar{\sigma}(\cdot)$ denotes the maximum singular value of (\cdot) , and $G_{py}(j\omega, K)$ is given in (7).

2.5. Problem Formulation

The control problem for the DFIG in Figure 1 is: fix the controller K in Equation (5) such that the corresponding augmented-state system (7) is asymptotically stabilized when $\Delta K = 0$, and with respect to a given scalar $\gamma > 0$, the H_∞ performance in the FF interval Ω_d satisfies

$$\|G_{py}(j\omega, K)\|_{\infty}^{\Omega_d} < \gamma$$

To address the formulated problem, the following lemmas will be exploited.

Lemma 1 ([21]). For the transfer function $G_{py}(s, K)$ in (8), if there exists a matrix $\Pi = \Pi^T$ such that

$$\begin{bmatrix} G_{py}^H(j\omega) & I \end{bmatrix} \Pi \begin{bmatrix} G_{py}(j\omega, K) \\ I \end{bmatrix} < 0, \forall \omega \in [\omega_1, \omega_2]$$

if and only if there exist matrices $P = P^T, X = X^T, Q = Q^T$ and $Z = Z^T$ satisfying

$$\begin{aligned} & \begin{bmatrix} A & B_2K & B_1 \\ I & 0 & 0 \end{bmatrix}^T (\Phi \otimes P + \Psi \otimes Q + \Psi_0 \otimes \tau_m Z) \begin{bmatrix} A & B_2K & B_1 \\ I & 0 & 0 \end{bmatrix} n \\ & + \begin{bmatrix} C & DK & 0 \\ 0 & 0 & I \end{bmatrix}^T \Pi \begin{bmatrix} C & DK & 0 \\ 0 & 0 & I \end{bmatrix} + \begin{bmatrix} X - \tau_m^{-1}Z & \tau_m^{-1}Z & 0 \\ \tau_m^{-1}Z & -X - \tau_m^{-1}Z & 0 \\ 0 & 0 & 0 \end{bmatrix} < 0 \end{aligned} \tag{9}$$

where

$$\Psi = \begin{bmatrix} -1 & j\omega_c \\ -j\omega_c & -\omega_1\omega_2 \end{bmatrix}, \Psi_0 = \begin{bmatrix} 1 & 0 \\ 0 & 0 \end{bmatrix}, \Phi = \begin{bmatrix} 0 & 1 \\ 1 & 0 \end{bmatrix}, \Pi = \begin{bmatrix} 1 & 0 \\ 0 & -\gamma^2 I \end{bmatrix}$$

In the above, $\omega_2 \geq \omega_1 > 0$ and $\omega_c = (\omega_1 + \omega_2)/2$ are used.

Lemma 2 (Projection Lemma [22]). For matrices $\Psi = \Psi^T, K$ and M , there exists a matrix X satisfying $\Psi + \text{He}(KXM) < 0$, if and only if $K^\perp \Psi K^{\perp T} < 0$ and $(M^T)^\perp \Psi (M^T)^\perp < 0$.

Lemma 3 (Jensen Inequality [23]). For any matrix $P = P^T > 0 \in R^n$, a scalar $\lambda > 0$, a vector function $\omega : [0, \lambda] \rightarrow R_n$ such that the following integrals are well-defined, then

$$\int_0^\lambda \omega^T(s) P \omega(s) ds \geq \left(\int_0^\lambda \omega(s) ds \right)^T P \left(\int_0^\lambda \omega(s) ds \right)$$

Lemma 4 ([23]). Given matrices $Q = Q^T, R, T$ of appropriate dimensions, we have

$$Q + RU(t)T + T^T U^T(t)R^T < 0, \forall t \geq 0 \tag{10}$$

for any $U(t)$ satisfying $U^T(t)U(t) < I$, if and only if there exists a scalar $\mu > 0$ such that

$$\begin{bmatrix} Q & \mu R & T^T \\ * & -\mu I & 0 \\ * & * & -\mu I \end{bmatrix} < 0 \quad (11)$$

Several remarks about **Lemmas 1 to 4**:

- Lemma 1 follows from the generalized Kalman–Yakubovich–Popov (GKYP) lemma, which is a frequency domain criterion that guarantees the existence of Lyapunov–Krasovskii functionals for stability analysis in nonlinear systems via strict positive realness in terms of transfer function [24,25]. In other words, the GKYP lemma provides us with time/frequency domain stability conditions. However, the LMI inequality of Lemma 1 must be interpreted in the time–domain fashion but related to some FF factors of the transfer function.
- The assumption that (A, B_1, C) is a minimal state–space realization of $G_{py}(s, K)$ is needed for generalizing the KYP lemma rigorously [26]. Thus, the pair (A, B_1) is controllable, and the pair (A, C) is observable.
- **Lemmas 2–4** can be interpreted both in the time and frequency domain ways. Confined to our discussion, they are used only in the time–domain fashion.
- The inequality (10) of Lemma 4 is a time–domain inequality. The equivalent inequality (11) should be interpreted also in the time–domain way if we retrieve the proof arguments between (10) and (11). The point plays a key role in combining the results in Lemmas 1 and 4.

3. FF H_∞ Controller Design of DFIG

In this section, a criterion of the FF H_∞ controller is presented for DFIGs with input time delay, which guarantees asymptotic stability and the desired H_∞ performance of the closed-loop DFIG system in (6). There will be four theorems to explain the controller design procedures, where the stability conditions in LMI are given in Section 3.1, LMIs under the harmonic interference attenuation condition are formulated in Section 3.2, and the H_∞ controller design and parametrization are provided in Section 3.3.

3.1. Stability Analysis

Theorem 1. For any delay $0 < \tau < \tau_m$, the closed-loop DFIG system (6) with $\Delta K = 0$ is asymptotically stable, if there exist a scalar $\alpha > 0$ and matrices $P_1 = P_1^T > 0$, $R_1 = R_1^T > 0$, $S_1 = S_1^T > 0$ and J such that the inequality $\Theta_1 < 0$ holds. Here, $\Theta_1 = \Theta_1^T$

$$\Theta_1 = \begin{bmatrix} \tau_m S_1 - \alpha \text{He}(J) & P_1 - \alpha J + \alpha J^T A & \alpha J^T B_2 K \\ * & R_1 - \tau_m^{-1} S_1 + \alpha \text{He}(A^T J) & \alpha J^T B_2 K + \tau_m^{-1} S_1 \\ * & * & -R_1 - \tau_m^{-1} S_1 \end{bmatrix} < 0 \quad (12)$$

The proof of Theorem 1 is given in Appendix A.1.

3.2. FF-Domain H_∞ Performance Analysis

Theorem 2. Let the FF interval Ω_d be defined in (8) and the delay $0 < \tau < \tau_m$ and a scalar $\gamma > 0$ be given. Then, the closed-loop DFIG system (6) with $\Delta K = 0$ satisfies the FF H_∞ performance inequality $\|G_{py}(s, K)\|_{\infty}^{\Omega_d} < \gamma$, if there exist matrices $P_2 = P_2^T > 0$, $Q_2 = Q_2^T > 0$, $X = X^T > 0$, $Z = Z^T > 0$ and J such that the inequality $\Theta_2 < 0$ holds. Here, $\Theta_2 = \Theta_2^T$ is given by

$$\Theta_2 = \begin{bmatrix} -Q_2 + \tau_m Z & P_2 + j\omega_c Q_2 - J & 0 & 0 & 0 \\ * & -\omega_1 \omega_2 Q_2 + \text{He}(A^T J) + X - \tau_m^{-1} Z & J^T B_2 K + \tau_m^{-1} Z & J^T B_1 & C^T \\ * & * & -X - \tau_m^{-1} Z & 0 & K^T D^T \\ * & * & * & -\gamma^2 I & 0 \\ * & * & * & * & -I \end{bmatrix} \quad (13)$$

The proof of Theorem 1 is given in Appendix A.2.

3.3. FF Controller Parametrization

It must be noticed that in Theorems 1 and 2, the gain disturbance ΔK is not considered. To enhance the stability robustness of the closed-loop system (6) against gain disturbance $\Delta K \neq 0$ by means of the practical controller $K + \Delta K$, the results of Theorems 1 and 2 must be modified. The following theorem can be obtained by using Lemma 4.

Theorem 3. For any time delay $0 < \tau < \tau_m$, there exists a controller (4) with gain disturbance $\Delta K = RU(t)TK$ constrained by (5) such that the closed-loop system (6) is asymptotically stabilized and satisfies the FF H_∞ performance, if there exist matrices $P_1 = P_1^T > 0$, $R_1 = R_1^T > 0$, $S_1 = S_1^T > 0$, $P_2 = P_2^T > 0$, $Q_2 = Q_2^T > 0$, $X = X^T > 0$, $Z = Z^T > 0$ and a general matrix J , the following LMIs holds true.

$$\Theta_3 = \Theta_3^T =: \begin{bmatrix} \phi_{11} & \phi_{12} & \phi_{13} & \phi_{14} & 0 \\ * & \phi_{22} & \phi_{23} & \phi_{24} & 0 \\ * & * & \phi_{33} & 0 & \phi_{35} \\ * & * & * & -\mu I & 0 \\ * & * & * & * & -\mu I \end{bmatrix} < 0 \quad (14)$$

$$\text{where} \begin{cases} \phi_{11} = \tau_m S_1 - \alpha \text{He}(J), & \phi_{12} = P_1 - \alpha J + \alpha J^T A \\ \phi_{13} = \alpha J^T B_2 K, & \phi_{14} = \mu \alpha J^T B_2 R \\ \phi_{22} = R_1 - \tau_m^{-1} S_1 + \alpha \text{He}(A^T J), & \phi_{23} = \alpha J^T B_2 K + \tau_m^{-1} S_1 \\ \phi_{24} = \phi_{14}, \phi_{33} = -R_1 - \tau_m^{-1} S_1, & \phi_{35} = K^T T^T \end{cases}$$

$$\Theta_4 = \Theta_4^T =: \begin{bmatrix} \Psi_{11} & \Psi_{12} & 0 & 0 & 0 & 0 & 0 \\ * & \Psi_{22} & \Psi_{23} & J^T B_1 & C^T & \mu J^T B_2 R & 0 \\ * & * & \Psi_{33} & 0 & K^T D^T & 0 & K^T T^T \\ * & * & * & -\gamma^2 I & 0 & 0 & 0 \\ * & * & * & * & -I & \mu DR & 0 \\ * & * & * & * & * & -\mu I & 0 \\ * & * & * & * & * & * & -\mu I \end{bmatrix} < 0 \quad (15)$$

$$\text{where} \begin{cases} \Psi_{11} = -Q_2 + \tau_m Z, \Psi_{12} = P_2 + j\omega_c Q_2 - J \\ \Psi_{22} = -\omega_1 \omega_2 Q_2 + \text{He}(A^T J) + X - \tau_m^{-1} Z \\ \Psi_{23} = J^T B_2 K + \tau_m^{-1} Z, \Psi_{33} = -X - \tau_m^{-1} Z \end{cases}$$

The proof of Theorem 1 is given in Appendix A.3.

Since the LMIs in (14) and (15) involve the product terms of K and J , they cannot be handled directly by means of the LMI numerical toolkit. To decouple such product terms, let us define

$$W_1 = \text{diag}[J^{-T}, J^{-T}, J^{-T}], W_2 = \text{diag}[J^{-T}, J^{-T}, J^{-T}, I, I]$$

Then, we pre- and post-multiply Equations (22) and (23) with W_1, W_1^T and W_2, W_2^T , respectively. Additionally, we introduce the notations as follows.

$$\begin{cases} \bar{P}_1 = J^{-T}P_1J^{-1}, \bar{R}_1 = J^{-T}R_1J^{-1}, \bar{S}_1 = J^{-T}S_1J^{-1} \\ \bar{P}_2 = J^{-T}P_2J^{-1}, \bar{Q}_2 = J^{-T}Q_2J^{-1}, \bar{Z} = J^{-T}ZJ^{-1} \\ \bar{X} = J^{-T}XJ^{-1}, V = KJ^{-1}, \bar{J} = J^{-1} \end{cases}$$

Using these notations, we can claim the following theorem.

Theorem 4. For any time delay $0 < \tau < \tau_m$, there exists a controller (4) with gain disturbance $\Delta K = RU(t)TK$ constrained by (5) such that the closed-loop system (6) is asymptotically stabilized and satisfies the FF H_∞ performance, if there exist matrices $\bar{P}_1 = \bar{P}_1^T > 0, \bar{R}_1 = \bar{R}_1^T > 0, \bar{S}_1 = \bar{S}_1^T > 0, \bar{P}_2 = \bar{P}_2^T > 0, \bar{Q}_2 = \bar{Q}_2^T > 0, \bar{X} = \bar{X}^T > 0, \bar{Z} = \bar{Z}^T > 0$ and a general matrix \bar{J}, V such that the following LMIs holds true.

$$\bar{\Theta}_3 = \bar{\Theta}_3^T =: \begin{bmatrix} \bar{\phi}_{11} & \bar{\phi}_{12} & \bar{\phi}_{13} & \bar{\phi}_{14} & 0 \\ * & \bar{\phi}_{22} & \bar{\phi}_{23} & \bar{\phi}_{24} & 0 \\ * & * & \bar{\phi}_{33} & 0 & \bar{\phi}_{35} \\ * & * & * & -\mu I & 0 \\ * & * & * & * & -\mu I \end{bmatrix} < 0 \tag{16}$$

$$\text{where } \begin{cases} \bar{\phi}_{11} = \tau_m \bar{S}_1 - \alpha \text{He}(\bar{J}), \bar{\phi}_{12} = \bar{P}_1 - \alpha \bar{J}^T + \alpha A \bar{J} \\ \bar{\phi}_{13} = \alpha B_2 V, \bar{\phi}_{14} = \mu \alpha B_2 R \\ \bar{\phi}_{22} = \bar{R}_1 - \tau_m^{-1} \bar{S}_1 + \alpha \text{He}(A \bar{J}), \bar{\phi}_{23} = \alpha B_2 V + \tau_m^{-1} \bar{S}_1, \bar{\phi}_{24} = \mu \alpha B_2 R \\ \bar{\phi}_{33} = -\bar{R}_1 - \tau_m^{-1} \bar{S}_1, \bar{\phi}_{35} = V^T T^T \end{cases}$$

$$\bar{\Theta}_4 = \bar{\Theta}_4^T =: \begin{bmatrix} \bar{\Psi}_{11} & \bar{\Psi}_{12} & 0 & 0 & 0 & 0 & 0 \\ * & \bar{\Psi}_{22} & \bar{\Psi}_{23} & B_1 & \bar{J}^T C^T & \mu B_2 R & 0 \\ * & * & \bar{\Psi}_{33} & 0 & V^T D^T & 0 & V^T T^T \\ * & * & * & -\gamma^2 I & 0 & 0 & 0 \\ * & * & * & * & -I & \mu DR & 0 \\ * & * & * & * & * & -\mu I & 0 \\ * & * & * & * & * & * & -\mu I \end{bmatrix} < 0 \tag{17}$$

$$\text{where } \begin{cases} \bar{\Psi}_{11} = -\bar{Q}_2 + \tau_m \bar{Z}, \bar{\Psi}_{12} = \bar{P}_2 + j\omega_c \bar{Q}_2 - \bar{J}^T \\ \bar{\Psi}_{22} = -\omega_1 \omega_2 \bar{Q}_2 + \text{He}(A \bar{J}) + \bar{X} - \tau_m^{-1} \bar{Z}, \bar{\Psi}_{23} = B_2 V + \tau_m^{-1} \bar{Z} \\ \bar{\Psi}_{33} = -\bar{X} - \tau_m^{-1} \bar{Z} \end{cases}$$

Moreover, the control gain K can be given by $K = V\bar{J}^{-1}$.

The FF H_∞ control for the DFIG flow chart is shown in Figure 3. control for DFIG flow chart.

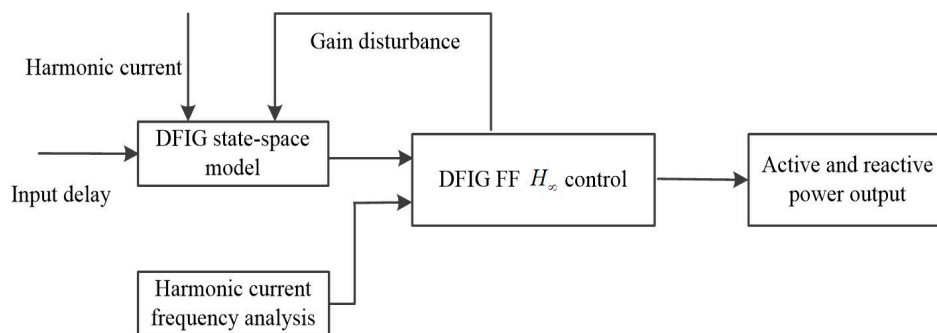


Figure 3. The FF H_∞ control for DFIG flow chart.

4. Numerical Simulations

In this section, we illustrate effectiveness of the suggested FF H_∞ control strategies.

4.1. Descriptions about DFIG and Control Design

The modeling parameters of the 5 MW wind turbine DFIGs are: $H = 6$ sec, $L_m = 0.4$ p.u., $L_{rr} = 0.55$ p.u., $L_{ss} = 0.17$ p.u., $R_r = 0.5$ p.u., $i_{ds0} = 1.8$ p.u., $i_{qs0} = 1.7$ p.u., $E_{ds0} = 2.8$ p.u., $E_{qs0} = 2.7$ p.u., $\omega_{r0} = 3.14$ p.u.. The linearized DFIG state–space equation matrices in the sense of (9) is given by

$$A = \begin{bmatrix} -2 & -0.15 & -0.14 \\ -2.7 & -1 & -2.14 \\ 2.8 & 2.14 & -1 \end{bmatrix}, B_1 = \begin{bmatrix} 0 & 0 \\ 0 & 0.3 \\ -0.3 & 0 \end{bmatrix},$$

$$B_2 = \begin{bmatrix} 0 & 0 \\ 0 & -0.7 \\ 0.7 & 0 \end{bmatrix}, C = \begin{bmatrix} 1 & 0 & 0 \\ 0 & 1.8 & 1.7 \\ 0 & -1.7 & 1.8 \end{bmatrix}, D = 0$$

The finite frequency domain interval of the current harmonic interference is first estimated as $2 \text{ kHz} < \omega_d < 8 \text{ kHz}$. We assume that $\tau_m = 100$ ms. Given $\alpha = 1$, $\gamma = 1$, $\mu = 0.3$, $R = 1$, $U = 1$, $T = 0.005$, we solve the corresponding LMIs (22) and (23) in Theorem 4. The FF controller K is fixed as

$$K = \begin{bmatrix} -1.859 & -0.570 & -2.250 \\ -1.368 & 1.986 & -1.392 \end{bmatrix}$$

The frequency characteristics for the maximum singular value of $G_{py}(s, K)$ is plotted in Figure 4. We see that the max value of $\|G_{py}(j\omega, K)\|$ is 0.283, which is strictly less than $\gamma = 1$.

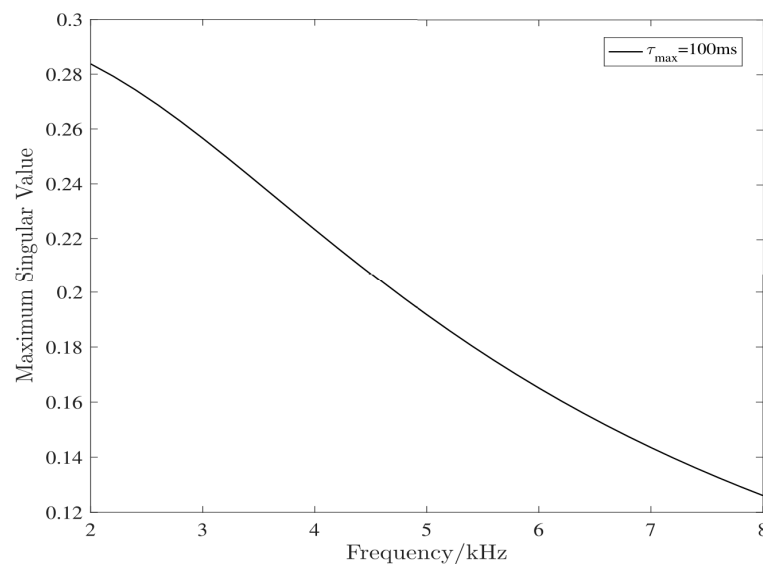


Figure 4. The maximum singular value plotting of $\|G_{py}(j\omega, K)\|$ over Ω_d .

Now we consider the cases subject to current harmonic interference. More specifically, the harmonic interference is in the form of $p(t) = 0.1 \sin(2\pi ft)$ ($f = 3$ kHz). The DFIG rotor angular velocity, the stator active and reactive power responses in the open-loop system (by dotted lines) and those in the closed-loop system (by solid lines) are plotted in Figure 5.

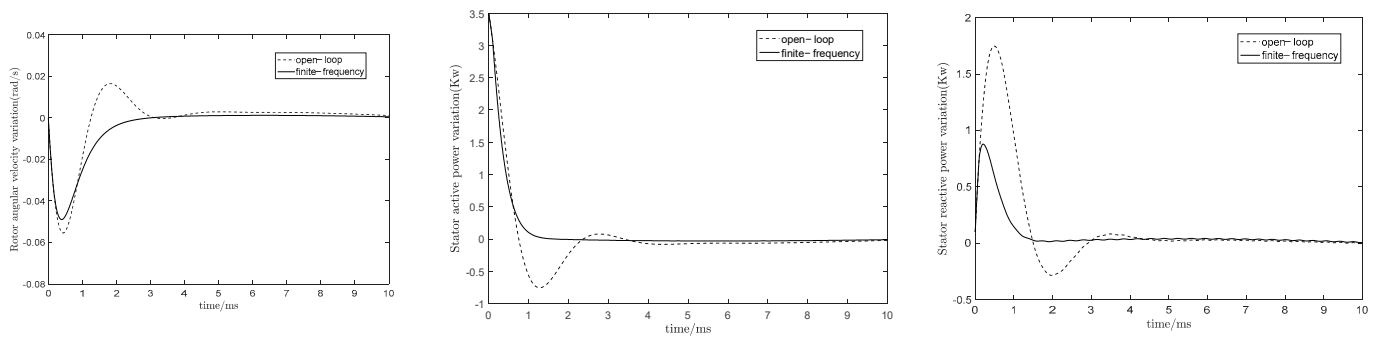


Figure 5. The response curves of the DFIG $\Delta\omega_r$, ΔP_s , ΔQ_s .

In Figure 5, we see that the oscillation amplitude of the closed-loop responses under the FF H_∞ control is smaller, and the response convergence is faster than that of the open-loop responses. It shows that the FF H_∞ controller reduces the transient time period while it stabilizes the closed-loop system.

4.2. Cases under Various Time Delays

To reveal how the time delay upper bound τ_m is related to the FF H_∞ performance, we made a comparison computation when $\tau_m \in \{100, 500, 1000, 1500\}$ ms, respectively. The H_∞ controller parametrization under different τ_m s are collected in Table 1. The response curves of the DFIG rotor angular velocity, stator active and reactive powers are plotted in Figure 6, where w.r.t. is the abbreviation for with respect to. By Figure 6, one can see that the larger the delay upper bound is, the worse (or the bigger) the resulting H_∞ performance index is.

Table 1. The Gain Matrix K under different τ_m s.

Delay/ms	Feedback Gain Matrix K	Feasibility
100	$K = \begin{bmatrix} -1.859 & -0.570 & -2.250 \\ -1.368 & 1.986 & -1.392 \end{bmatrix}$	✓
500	$K = \begin{bmatrix} -0.199 & -0.075 & -0.280 \\ -0.808 & 0.586 & -0.265 \end{bmatrix}$	✓
1000	$K = \begin{bmatrix} -0.243 & -0.3 & 0.330 \\ -0.741 & -0.199 & -0.272 \end{bmatrix}$	✓
1500	$K = \begin{bmatrix} -0.619 & -0.542 & 0.212 \\ -0.702 & -0.217 & -0.503 \end{bmatrix}$	✓

4.3. Cases under Various Gain Disturbances

To illustrate how the gain perturbation ΔK affects the control performance, we selected $R = 1$, $U = 1$, and the weighting factor $T \in \{0.005, 0.05, 0.5\}$, respectively. Substituting R , U , T into the Equation (5), we obtained the corresponding $\Delta K \in \{0.005K, 0.05K, 0.5K\}$. Then, we compared the control performances under different ΔK . The H_∞ controller gain matrix K are listed in Table 2. The response curves of DFIG rotor angular velocity, stator active and reactive powers are plotted in Figure 7. By Figure 7, it is easy to deduce that as the control gain perturbation ΔK grows, the corresponding H_∞ performance deteriorates obviously.

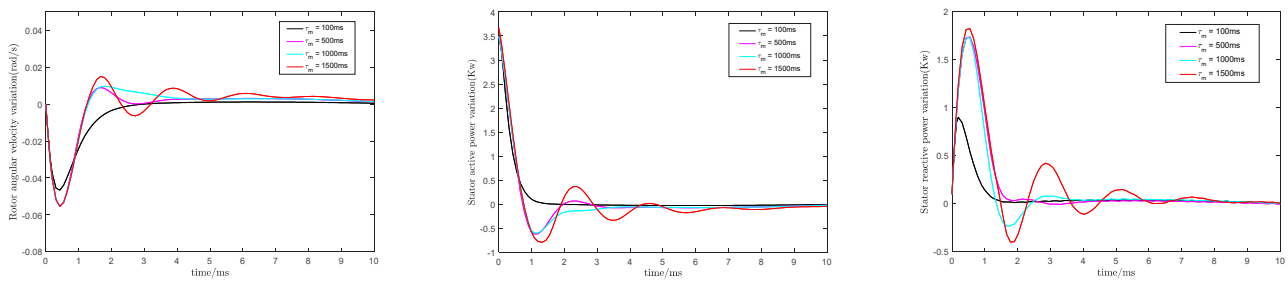


Figure 6. The response curves of the DFIG $\Delta\omega_r$, ΔP_s , ΔQ_s w.r.t. τ_m .

Table 2. The Gain Matrix K under different ΔK .

ΔK	Feedback Gain Matrix K	Feasibility
0.005 K	$K = \begin{bmatrix} -1.859 & -0.57 & -2.25 \\ -1.368 & 1.986 & -1.392 \end{bmatrix}$	✓
0.05 K	$K = \begin{bmatrix} -1.816 & -0.533 & -2.197 \\ 1.312 & 1.949 & -1.342 \end{bmatrix}$	✓
0.5 K	$K = \begin{bmatrix} -0.152 & -0.047 & -0.145 \\ -0.025 & 0.12 & -0.071 \end{bmatrix}$	✓

4.4. Cases for Various Finite Frequency Domain Intervals

To reveal the H_∞ control performance under different current harmonic frequency interval $\Omega_d s$, we evaluate several when $\Omega_d \in \{[50, 150] \text{Hz}, [250, 550] \text{Hz}, [2000, 8000] \text{Hz}\}$. The corresponding H_∞ controller parametrizations for different Ω_d are listed in Table 3. The response curves of DFIG rotor angular velocity, stator active and reactive powers are plotted in Figure 8. From Figure 8, we can see that the H_∞ control can well suppress the current harmonics interference in all three cases. This verifies the effectiveness and robustness of the suggested controller.

4.5. Cases Comparison under FF and EF H_∞ Control

Finally, we compared the H_∞ control performances in the finite frequency (FF) sense with those in the entire-frequency (EF) sense. In Figure 9, the dotted lines and the solid lines, respectively, represent the response curves of the DFIG power systems under the FF H_∞ and EF H_∞ control. Clearly, the response curves related to the FF H_∞ controller are smoother, while the overshoots are less, and thus the control performance under the FF H_∞ control is significantly enhanced.

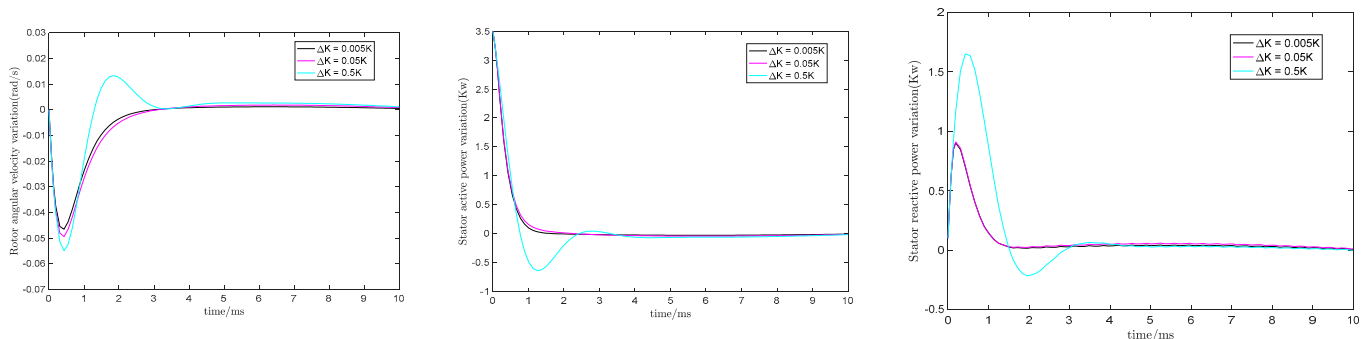


Figure 7. The response curves of the DFIG $\Delta\omega_r$, ΔP_s , ΔQ_s w.r.t. ΔK .

Table 3. The Gain Matrix K under different Ω_d s.

Ω_d/Hz	Feedback Gain Matrix K	Feasibility
$50 < \Omega_d < 150$	$K = \begin{bmatrix} -2.27 & -0.884 & -2.137 \\ -1.657 & 1.688 & -1.676 \end{bmatrix}$	✓
$250 < \Omega_d < 550$	$K = \begin{bmatrix} -1.908 & -0.575 & -2.5714 \\ -1.569 & 2.523 & -1.508 \end{bmatrix}$	✓
$2000 < \Omega_d < 8000$	$K = \begin{bmatrix} -1.859 & -0.570 & -2.25 \\ -1.368 & 1.986 & -1.392 \end{bmatrix}$	✓

4.6. Cases Comparison under FF and Other H_∞ Control Methods

Finally, for comparison, the FF H_∞ control method in this paper and the general H_∞ control method in the literature [27] are applied in this example where parameters are chosen as $\tau_m = 100\text{ms}$, $\Delta K = 0.005K$. It is evident from Figure 10 that the control performance under the FF H_∞ control proposed in this paper is significantly improved compared to the ones in the literature [27].

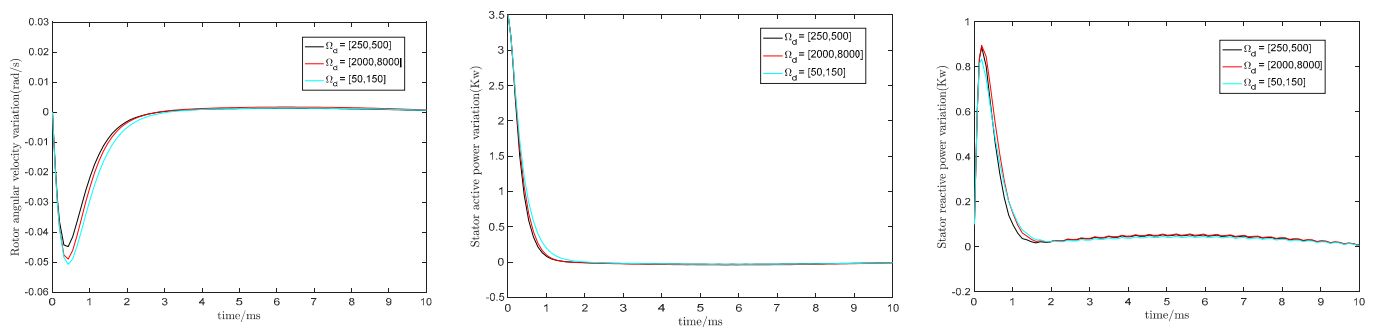


Figure 8. The response curves of the DFIG $\Delta\omega_r$, ΔP_s , ΔQ_s w.r.t. Ω_d .

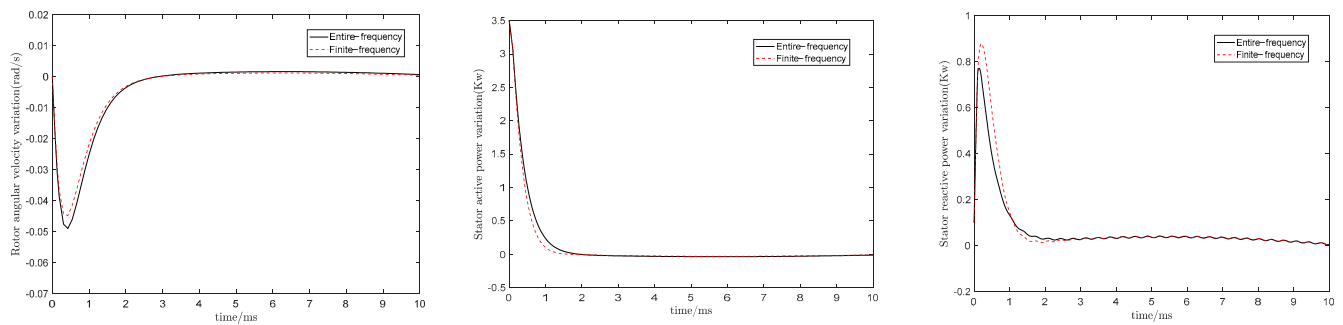


Figure 9. The response curves of the DFIG $\Delta\omega_r$, ΔP_s , ΔQ_s under FF and EF.

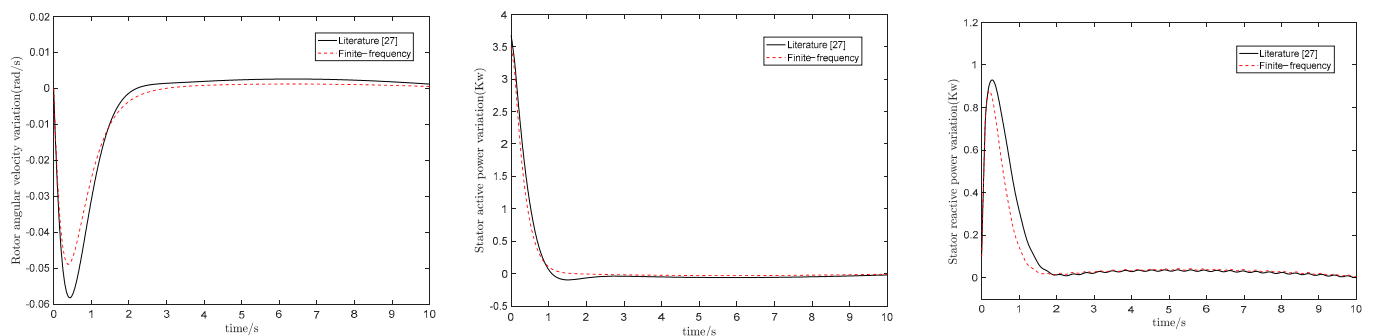


Figure 10. The response of the DFIG $\Delta\omega_r$, ΔP_s , ΔQ_s under two methods.

5. Discussions

In this paper, a state-feedback control scheme is proposed, which caters for the FF control problem for the DFIG system with the time delay, current harmonics and gain disturbances. This method is of great significance in improving the robustness of wind power systems.

The third order DFIG turbine model adopts a one-mass drive and ignores the stator transient, so some flux components are not responsible for the turbine's decaying and oscillating modes. This model is more suitable for real DFIG systems. Then the state-space model for DFIGs was obtained using Taylor's formula.

In large power systems, electricity may oscillate in a short period of time due to time delays, which reflects badly on turbines, power equipment and the power grid. The harmonic interferences and gain disturbances in the power system can reduce the power quality, leading to lower generation efficiency and higher generation costs for wind farms. It is necessary to study the time delay control of large-scale wind power systems under current harmonic disturbances and gain disturbances.

For the DFIG state-space model with input delay under current harmonics and gain disturbances model, an FF H_∞ state-feedback controller was designed from the frequency domain perspective, which makes the DFIG stable and robust against harmonic interferences and gain disturbances. Using the generalized KYP lemma and Lyapunov theory, the FF performance was evaluated using linear matrix inequalities, and the state feedback parametrization was addressed based on this. This method improves the utilization rate of wind energy and is a feasible and effective control method in wind power systems.

In summary, the method proposed in this paper is technically and economically advantageous in terms of power generation performance, system simplification and cost-effectiveness. A new control technology and system structure were applied to analyze power systems and improve the power quality.

Potential applications of the method are as follows.

- At present, the control technology of wind power technology is relatively mature. The FF H_∞ control design method in this paper provides a new frequency domain design idea for the suppression of disturbances in various uncertain cases of wind power systems, which can improve the quality of power systems.
- With the development of distributed wind power systems in wind farms, the distributed wind turbines based on FF H_∞ control for doubly fed induction generators with input delay and the gain disturbance control strategy proposed in this paper could be used in wind farms, which can realize the efficient use of wind energy.

6. Conclusions

In view of DFIG wind turbine systems, the FF H_∞ control method was proposed for systems with input delay under controller gain disturbance and current harmonic interference. By employing the GKYP lemma and Lyapunov theory, the FF H_∞ control problem can be transformed into an LMI feasible solution problem. Interesting results are claimed as in Theorems 1–4. The main contributions and novelty of the proposed methods in this paper can be summarized by the following aspects:

1. A control strategy in terms of the frequency band is formulated for the DFIG by taking time delay and gain disturbance into account, and it has not been fully considered in previous studies on the control of the DFIG.
2. Based on the GKYP lemma and the Lyapunov theory, sufficient conditions are formulated for the DFIG with input delay to satisfy the desired specification in the frequency band. Then, the frequency design problem of DFIGs is transformed into a time domain LMI problem, which significantly facilitated our solution process.
3. A sufficient condition is presented to search for the optimal FF controller for the DFIG. Furthermore, the output of active and reactive power was stable, which improved the stability and reliability of the system. This design method provided new ideas for the development and application of DFIG control in the future.

As possible extensions of the FF LMI technique in DFIG engineering, the following control problems are significant and interesting, which will be addressed in our subsequent studies.

- The model for DFIGs in this paper is 3-dimensional. Next, higher order systems with higher dimensional DFIG systems can be considered [28,29].
- Sliding mode control: $u(t) = f(t, x(t), x(t - \tau))$ over a sliding surface $S(t, x(t), x(t - \tau))$ can be applied to achieve finite-time convergence.
- Apply the results for networked DFIGs via multi-agent consensus [30–32].

Author Contributions: S.W. contributed to the design, analysis, and writing of the paper. J.Z. analyzed the data and performed the computer simulations. Z.D. contributed to give some suggestions and consultation. All authors have read and agreed to the published version of the manuscript.

Funding: This research received no external funding.

Institutional Review Board Statement: Not applicable.

Informed Consent Statement: Not applicable.

Data Availability Statement: Not applicable.

Conflicts of Interest: The authors declare no conflict of interest.

Appendix A

Appendix A.1

Proof of Theorem 1. By simple algebras, the inequality (12) is written as

$$\Theta_1 = \begin{bmatrix} \tau_m S_1 & P_1 & 0 \\ * & 0 & 0 \\ * & * & 0 \end{bmatrix} + \begin{bmatrix} 0 & 0 & 0 \\ * & R_1 - \tau_m^{-1} S_1 & \tau_m^{-1} S_1 \\ * & * & -R_1 - \tau_m^{-1} S_1 \end{bmatrix} + \begin{bmatrix} -\alpha \text{He}(J) & -\alpha J + \alpha J^T & \alpha J^T B_2 K \\ * & \alpha \text{He}(A^T J) & \alpha J^T B_2 K \\ * & * & 0 \end{bmatrix} < 0$$

Furthermore, let us define the following notations:

$$\begin{cases} G_1 = \begin{bmatrix} I & 0 & 0 \\ 0 & I & 0 \end{bmatrix}, M_1 = \begin{bmatrix} 0 & 0 & 0 \\ * & R_1 - \tau_m^{-1} S_1 & \tau_m^{-1} S_1 \\ * & * & -R_1 - \tau_m^{-1} S_1 \end{bmatrix} \\ \Delta_1 = \begin{bmatrix} -I & A & B_2 K \end{bmatrix}, \nabla_1 = \begin{bmatrix} I & I & 0 \end{bmatrix} \end{cases}$$

Then, the inequality (12) can be transformed into the following relationship.

$$G_1^T (\Phi \otimes P_1 + \Psi_0 \otimes \tau S_1) G_1 + M_1 + \alpha \text{He}(\Delta_1^T J \nabla_1) < 0 \quad (\text{A1})$$

where Φ and Ψ are defined in Lemma 1.

By Lemma 2, the inequality (A1) holds if and only if the following inequalities are true.

$$\begin{cases} L_1 G^T (\Phi \otimes P_1 + \Psi_0 \otimes \tau_m S_1) G_1 L_1^T + L_1 M_1 L_1^T < 0 \\ D_1 G_1^T (\Phi \otimes P_1 + \Psi_0 \otimes \tau_m S_1) G_1 D_1^T + D_1 M_1 D_1^T < 0 \end{cases} \quad (\text{A2})$$

where

$$D_1 = \begin{bmatrix} A & B_2 K \\ I & 0 \\ 0 & I \end{bmatrix}, L_1 = \begin{bmatrix} 0 & 0 & 0 \\ 0 & 0 & I \end{bmatrix}$$

Furthermore, the second inequality of (A2) can be transformed into

$$\begin{aligned}
 & D_1^T G_1^T (\Phi \otimes P_1 + \Psi_0 \otimes \tau_m S_1) G_1 D_1 + D_1^T M_1 D_1 \\
 &= \begin{bmatrix} A & B_2 K \\ I & 0 \end{bmatrix}^T (\Phi \otimes P_1 + \Psi_0 \otimes \tau_m S_1) \begin{bmatrix} A & B_2 K \\ I & 0 \end{bmatrix} \\
 & \quad + \begin{bmatrix} R_1 - \tau_m^{-1} S_1 & \tau_m^{-1} S_1 \\ * & -R_1 - \tau_m^{-1} S_1 \end{bmatrix} < 0
 \end{aligned} \tag{A3}$$

Substituting Φ, Ψ_0 into the above equation, we obtain

$$\begin{bmatrix} \text{He}(A^T P_1) + R_1 + \tau_m A^T S_1 A - \tau_m^{-1} S_1 & P_1 B_2 K + \tau_m A^T S_1 B_2 K + \tau_m^{-1} S_1 \\ * & -R_1 + \tau_m K^T B_2^T S_1 B_2 K - \tau_m^{-1} S_1 \end{bmatrix} < 0 \tag{A4}$$

It follows that the Equation (A4) is equivalent to the Equation (12).

Next we construct the Lyapunov–Krasovskii functional $V(t)$ for stability analysis of the system (6) when no current harmonic interference $p(t)$ and gain disturbance $\Delta K = 0$ are assumed.

$$V(t) = V_1(t) + V_2(t) + V_3(t)$$

where

$$\begin{cases} V_1(t) = x^T(t) P_1 x(t), & V_2(t) = \int_{t-\tau}^t x^T(\xi) R_1 x(\xi) d\xi \\ V_3(t) = \int_{-\tau}^0 \int_{t+\beta}^t \dot{x}^T(\xi) S_1 \dot{x}(\xi) d\xi d\beta \end{cases}$$

After taking the time derivative about $V(t)$, we obtain that

$$\begin{aligned}
 \dot{V}(t) &= \dot{x}(t)^T P_1 x(t) + x^T(t) P_1 \dot{x}(t) + x^T(t) R_1 x(t) - x^T(t - \tau) R_1 x(t - \tau) \\
 & \quad + \tau \dot{x}^T(t) S_1 \dot{x}(t) - \int_{t-\tau}^t \dot{x}^T(\beta) S_1 \dot{x}(\beta) d\beta
 \end{aligned} \tag{A5}$$

By Lemma 4, the last term of Equation (A5) can be scaled up to

$$- \int_{t-\tau}^t \dot{x}^T(\beta) S_1 \dot{x}(\beta) d\beta \leq -\tau^{-1} (x(t) - x(t - \tau))^T S_1 (x(t) - x(t - \tau)) \tag{A6}$$

Substituting the Equation (A6) and $\dot{x}(t) = Ax(t) + B_2 Kx(t - \tau)$ into the Equation (A5), we have

$$\begin{aligned}
 \dot{V}(t) &\leq \dot{x}(t)^T P_1 x(t) + x^T(t) P_1 \dot{x}(t) + x^T(t) R_1 x(t) \\
 & \quad - x^T(t - \tau) R_1 x(t - \tau) + \tau_m \dot{x}^T(t) S_1 \dot{x}(t) \\
 & \quad - \tau_m^{-1} (x(t) - x(t - \tau))^T S_1 (x(t) - x(t - \tau)) \\
 & = \zeta^T \Sigma \zeta
 \end{aligned}$$

where the vector ζ and the matrix $\Sigma = \Sigma^T$ are defined by

$$\begin{cases} \zeta = \begin{bmatrix} x(t) \\ x(t - \tau) \end{bmatrix} \\ \Sigma = \begin{bmatrix} \text{He}(A^T P_1) + R_1 + \tau_m A^T S_1 A - \tau_m^{-1} S_1 & P_1 B_2 K + \tau_m A^T S_1 B_2 K + \tau_m^{-1} S_1 \\ * & -R_1 + \tau_m K^T B_2^T S_1 B_2 K - \tau_m^{-1} S_1 \end{bmatrix} \end{cases}$$

Together with Schur lemma, if $\Sigma = \Sigma^T < 0$, the closed-loop DFIG system is asymptotically stable. Since the inequality $\Sigma = \Sigma^T < 0$ is equivalent to that in (A4). Therefore, under the inequality (12), the closed-loop DFIG system is asymptotically stable. This completes the proof. \square

Appendix A.2

Proof of Theorem 2. Define the following notations:

$$\begin{cases} G_2 = \begin{bmatrix} I & 0 & 0 & 0 \\ 0 & I & 0 & 0 \end{bmatrix}, F_2 = \begin{bmatrix} 0 & C & DK & 0 \\ 0 & 0 & 0 & I \end{bmatrix} \\ M_2 = \begin{bmatrix} 0 & 0 & 0 & 0 \\ * & X - \tau_m^{-1}Z & \tau_m^{-1}Z & 0 \\ * & * & -X - \tau_m^{-1}Z & 0 \\ * & * & * & 0 \end{bmatrix} \\ \Delta_2 = \begin{bmatrix} -I & A & B_2K & B_1 \end{bmatrix}, \nabla_1 = \begin{bmatrix} 0 & I & 0 & 0 \end{bmatrix} \end{cases}$$

Then, the inequality $\Theta_2 < 0$ can be transformed into the following relationship.

$$G_2^T(\Phi \otimes P_2 + \Psi \otimes Q_2 + \Psi_0 \otimes \tau S_1)G_2 + F_2^T \Pi F_2 + M_2 + \text{He}(\Delta_2^T J \nabla_2) < 0. \quad (\text{A7})$$

By Lemma 2, the inequality (A7) holds if and only if the following inequalities are true.

$$\begin{cases} L_2^T G_2^T (\Phi \otimes P_2 + \Psi \otimes Q_2 + \Psi_0 \otimes \tau_m S_1) G_2 L_2^T + L_2^T F_2^T \Pi F_2 L_2 + L_2^T M_2 L_2 < 0 \\ D_2^T G_2^T (\Phi \otimes P_2 + \Psi \otimes Q_2 + \Psi_0 \otimes \tau_m S_1) G_2 D_2^T + D_2^T F_2^T \Pi F_2 D_2 + D_2^T M_2 D_2 < 0 \end{cases} \quad (\text{A8})$$

where

$$D_2 = \begin{bmatrix} A & B_2K & B_1 \\ I & 0 & 0 \\ 0 & I & 0 \\ 0 & 0 & I \end{bmatrix}^T, L_1 = \begin{bmatrix} I & 0 & 0 & 0 \\ 0 & I & I & 0 \end{bmatrix}$$

Furthermore, the second inequality of (A8) can be transformed into

$$\begin{aligned} & \begin{bmatrix} A & B_2K & B_1 \\ I & 0 & 0 \end{bmatrix}^T (\Phi \otimes P + \Psi \otimes Q + \Psi_0 \otimes \tau_m Z) \begin{bmatrix} A & B_2K & B_1 \\ I & 0 & 0 \end{bmatrix} \\ & + \begin{bmatrix} C & DK & 0 \\ 0 & 0 & I \end{bmatrix}^T \Pi \begin{bmatrix} C & DK & 0 \\ 0 & 0 & I \end{bmatrix} + \begin{bmatrix} X - \tau_m^{-1}Z & \tau_m^{-1}Z & 0 \\ \tau_m^{-1}Z & -X - \tau_m^{-1}Z & 0 \\ 0 & 0 & 0 \end{bmatrix} < 0 \end{aligned}$$

which is nothing but the inequality (9). Eventually, by Lemma 1, the inequality $\Theta_2 < 0$ implies that $G_{py}^H(j\omega)G_{py}(j\omega, K) < \gamma^2 I$. This gives the inequality $\|G_{py}(j\omega, K)\|_\infty^{\Omega_d} < \gamma$. This completes the proof. \square

Appendix A.3

Proof of Theorem 3. By replacing K with $K + RU(t)TK$ in the inequalities (12) and (13), the inequalities (12) and (13), respectively, can be modified as

$$\begin{cases} \Theta_1 + R_1 U(t) T_1 + T_1^T U^T(t) R_1^T < 0 \\ \Theta_2 + R_2 U(t) T_2 + T_2^T U^T(t) R_2^T < 0 \end{cases} \quad (\text{A9})$$

where

$$\begin{cases} R_1 = \begin{bmatrix} \mu \alpha J^T B_2 R \\ \mu \alpha J^T B_2 R \\ 0 \end{bmatrix}, T_1 = [0 \ 0 \ TK] \\ R_2 = \begin{bmatrix} \mu J^T B_2 R \\ 0 \\ 0 \\ \mu DR \end{bmatrix}, T_2 = [0 \ 0 \ TK \ 0 \ 0] \end{cases}$$

According to Lemma 4, the two inequalities of (A9) will be satisfied if there is a scalar $\mu > 0$ that makes the inequalities (14) and (15) be true. Bearing the facts in mind, Theorems 1 and 2 lead us to the desired results as appropriate. This completes the proof. \square

References

1. Trongtorkarn, M.; Theppaya, T.; Techato, K.; Luengchavanon, M.; Kasagepongsarn, C. Relationship between starting torque and thermal behavior for a permanent magnet synchronous generator (PMSG) applied with vertical axis wind Turbine (VAWT). *Sustainability* **2021**, *13*, 9151. [[CrossRef](#)]
2. Cady, S.T.; Dominguez-Garcia, A.D.; Hadjicostis, C.N. A Distributed Generation Control Architecture for Islanded AC Microgrids. *IEEE Trans. Control Syst. Technol.* **2015**, *23*, 1717–1735. [[CrossRef](#)]
3. Ekanayake, J.B.; Holdsworth, L.; Jenkins, N. Comparison of 5th order and 3rd order machine models for doubly-fed induction generator (DFIG) wind turbines. *Electr. Power Syst. Res.* **2003**, *67*, 207–215. [[CrossRef](#)]
4. Badihi, H.; Zhang, Y.M.; Hong, H. Wind turbine fault diagnosis and fault-tolerant torque load control against actuator faults. *IEEE Trans. Control Syst. Technol.* **2015**, *23*, 1351–1372. [[CrossRef](#)]
5. Tang, Z.; Wang, B.; Gao, X.; Liu, W.Y. L_2 disturbance suppression controller design for multiple time delays offshore wind turbines. *IEEE Access* **2020**, *8*, 92141–92152. [[CrossRef](#)]
6. Li, W.J.; Yin, M.H.; Chen, Z.Y.; Zou, Y. Inertia compensation scheme for wind turbine simulator based on deviation mitigation. *J. Mod. Power. Syst. Cle.* **2017**, *5*, 228–238. [[CrossRef](#)]
7. Xu, Z.Y.; Zhen, Q.; Qian, H.; Xu, Z.; Jing, Q.S. Impact of large-scale integrated wind farms on the small signal stability of power system. *Adv. Mater.* **2013**, *805*, 393–396. [[CrossRef](#)]
8. Wang, Z.; Sun, Y.Z.; Li, G.J.; Li, Z.G. Stator current harmonics analysis of doubly-fed induction generator. *Electric. Power Auto. Equip.* **2010**, *30*, 1–5.
9. Li, Q.L.; Zhang, B.; Liu, Y.B.; Tao, S.; Xu, Y.H. Ultra high harmonic transmission feature analysis of wind power generation. *Power Capacit. React. Power Compens.* **2020**, *41*, 171–179.
10. Sengamalai, U.; Thamizh Thentral, T.M.; Ramasamy, P.; Bajaj, M.; Bukhari, S.S.H.; Elattar, E.E.; Althobaiti, A.; Kamel, S. Mitigation of circulating bearing current in induction motor drive using modified ANN based MRAS for Traction Application. *Mathematics* **2022**, *10*, 1220. [[CrossRef](#)]
11. Kheshti, M.; Kang, X.N.; Song, G.B.; Jiao, Z.B. Modeling and fault analysis of doubly fed induction generators for gansu wind farm application. *Can. J. Electr. Comput. Eng.* **2015**, *38*, 52–64. [[CrossRef](#)]
12. Benbouzid, M.; Beltran, B.; Amirat, Y. Second-order sliding mode control for DFIG-based wind turbines fault ride-through capability enhancement. *ISA Trans.* **2014**, *53*, 827–833. [[CrossRef](#)] [[PubMed](#)]
13. Verwaa, N.W.; Veen, G.J.; Wingerden, J.W. Predictive control of an experimental wind turbine using preview wind speed measurements. *Wind. Energy* **2015**, *18*, 385–398. [[CrossRef](#)]
14. Takahashi, K.; Jargalsaikhan, N.; Rangarajan, S.; Hemeida, A.M. Output control of three-axis PMSG wind turbine considering torsional vibration using h infinity control. *Energies* **2020**, *13*, 3474. [[CrossRef](#)]
15. Kannan, K.; Sutha, P. PI-CCC based switched reluctance generator applications for wind power generation using MATLAB/SIMULINK. *J. Electr. Eng. Technol.* **2013**, *8*, 230–237.
16. Prasad, R.M.; Mulla, M.A. Control of DFIG wind turbine with direct-current vector control Configuration. *IEEE T. Sustain. Energ.* **2013**, *3*, 1–11.
17. Madanzadeh, S.; Bukhari, S.S.H.; Ro, J.S. Direct torque control of rotor-tied witch out rotor position sensor. *Int. J. Elec. Power* **2020**, *40*, 29–35.
18. Wu, F.; Zhang, X.P.; Ju, P.; Sterling, M.J. Decentralized nonlinear control of wind turbine with doubly fed induction generator. *IEEE Trans. Power Syst.* **2008**, *23*, 613–621.
19. Ackermann, T. *Wind Power in Power Systems*; John Wiley & Sons, Ltd.: Hoboken, NJ, USA, 2005; pp. 154–196.
20. Mirzajani, S.; Aghababa, M.; Heydari, A. Adaptive T-S fuzzy control design for fractional-order systems with parametric uncertainty and input constraint. *Fuzzy Set. Syst.* **2019**, *365*, 22–39. [[CrossRef](#)]
21. Zhang, X.N.; Yang, G.H. Performance analysis for multi-delay systems in finite frequency domains. *Int. J. Robust Nonlin.* **2012**, *22*, 933–944. [[CrossRef](#)]
22. Apkarian, P.; Tuan, H.D.; Bernussou, J. Continuous-time analysis, eigen structure assignment, and H_2 synthesis with enhanced linear matrix inequalities (LMI) characterizations. *IEEE Trans. Automat. Contr.* **2001**, *46*, 1941–1946. [[CrossRef](#)]
23. Cao, Y.Y.; Lam, J.; Sun, Y.X. Static output feedback stabilization: An ILMI approach. *Automatica* **1998**, *34*, 1641–1645. [[CrossRef](#)]
24. Haddad, W.M.; Chellaboina, V. *Nonlinear Dynamical Systems and Control—A Lyapunov-Based Approach*; Princeton University Press: Princeton, NJ, USA; Oxford, UK, 2008; pp. 164–172.
25. Wu, M.; He, Y.; She, J.H.; Liu, G.P. Delay-dependent criteria for robust stability of time-varying delay systems. *Automatica* **2004**, *40*, 1435–1439. [[CrossRef](#)]
26. Gao, H.; Sun, H.; Shi, P. Robust sampled-data H_∞ control for vehicle active suspension systems. *IEEE Trans. Control Syst. Technol.* **2010**, *18*, 238–245. [[CrossRef](#)]
27. Hui, J.J.; Zhang, H.X.; Kong, X.Y. Delay-dependent non-fragile H_∞ control for linear systems with interval time-varying delay. *Int. J. Autom. Comput.* **2011**, *12*, 109–116. [[CrossRef](#)]

28. Sun, B.; Ju, P.; Shahidehpour, M.; Pan, X. Calculation of stable domain of DFIG-based wind farm in series compensated power systems. *IEEE Access* **2020**, *8*, 34900–34908. [[CrossRef](#)]
29. Jia, Y.; Huang, T.; Li, Y.; Ma, R. Parameter setting strategy for the controller of the DFIG wind turbine considering the small-signal stability of power grids. *IEEE Access* **2020**, *8*, 31287–31294. [[CrossRef](#)]
30. Zhou, J.; Wang, C.; Qian, H.M. Existence, properties and trajectory specification of generalized multi-agent flocking. *Int. J. Control* **2017**, *92*, 1434–1456. [[CrossRef](#)]
31. Wang, C.; Zhou, J. Multi-agent collision approach for stabilizing multi-machine power networks with distributed excitation systems. *Ifac. J. Syst. Control* **2018**, *5*, 11–21. [[CrossRef](#)]
32. Zhou, J.; Li, X.L.; Huang, H.Q. Manifold consensus of multi-machine power networks by augmented multi-agent collision control and distributed implementation. *Int. J. Control* **2021**, *94*, 1434–1447. [[CrossRef](#)]

Disclaimer/Publisher’s Note: The statements, opinions and data contained in all publications are solely those of the individual author(s) and contributor(s) and not of MDPI and/or the editor(s). MDPI and/or the editor(s) disclaim responsibility for any injury to people or property resulting from any ideas, methods, instructions or products referred to in the content.